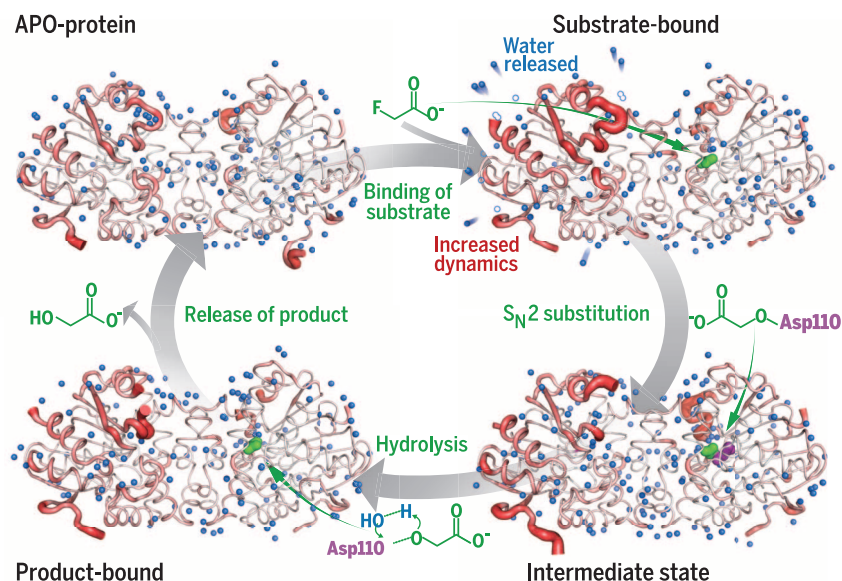## RESEARCH ARTICLE SUMMARY

ENZYME DYNAMICS

The role of dimer asymmetry and protomer dynamics in enzyme catalysis

Tae Hun Kim,* Pedram Mehrabi,* Zhong Ren, Adnan Sljoka, Christopher Ing, Alexandr Bezginov, Libin Ye, Régis Pomès, R. Scott Prosser,†‡ Emil F. Pai†‡

INTRODUCTION: Enzymes greatly accelerate biochemical reactions by providing a scaffold to bind and recognize substrate, position catalytic units, and facilitate the formation of stabilized transition states. The conformations associated with specific states along the reaction coordinate pathway are often observed to be sampled by the enzyme through a conformational selection mechanism. An enzyme-catalyzed reaction is not a simple linear process of discrete steps where the protein progresses in an ordered and sequential fashion. Rather, a more appropriate description is in terms of an ensemble of functional conformations. Here, we consider how such ensembles might function in the homodimeric enzyme fluoroacetate dehalogenase (FAcD) from *Rhodopseudomonas palustris*. Even under gross excess of substrate, this enzyme turns over only one substrate molecule at a time, raising the question of the role played by the dimer in catalysis.

Our results indicate that substrate binding to one protomer is allosterically communicated to the empty protomer, which plays a critical role in facilitating catalysis through entropic changes manifesting in enhanced dynamics and the loss of bound water molecules. Several key mutants were prepared so that the enzyme could also be studied in various stages associated with catalysis (i.e. substrate-free, Michaelis intermediate, covalent intermediate, and product-bound state). By characterizing these functional states using x-ray crystallography and solution-state nuclear magnetic resonance (NMR), it became possible to invoke an ensemble description of the enzyme at key points along the reaction. Interconversion between conformers and the dynamic allosteric processes associated with driving catalysis in the enzyme could be studied largely through ^{19}F NMR experiments, whereas the dynamic ensemble and key allosteric processes were validated by molecular dynamics (MD) simulations and computational rigidity analysis.

RATIONALE: Catalytic turnover numbers for most enzymes are between 1 and 10^4 s^{-1}. FAcD turnover, however, is conveniently slow (several substrate molecules per minute), making it feasible to interrogate functional states associated with unidirectional catalysis by means of freeze-trapping x-ray crystallography and NMR. Our goal was to investigate key functional mutants in order to derive an ensemble representation of the enzyme and to better understand how this ensemble achieves catalysis. The work provides new insights into the role of allostery and protein dynamics in catalysis, and in particular, how this takes place in a dimeric enzyme.

RESULTS: Crystallographic analysis identifies a subtle asymmetry in the dimer, where only one protomer is poised for substrate binding at any instance. NMR reveals that the two protomers undergo conformational exchange on a millisecond time scale. In the absence of substrate,

however, 0.5% of the enzyme molecules adopt an asymmetric ligand bound–like excited state with little or no conformational exchange. Upon binding of substrate, the asymmetry becomes more pronounced, and the empty protomer contributes to catalysis by shedding water molecules and adopting greater short–time scale fluctuations, thereby compensating for entropy losses associated with binding. In addition, conformational exchange between protomers markedly increases once the substrate is locked into the binding cleft. Substrate binding also initiates sampling of the covalent intermediate, and subsequent functional states on a millisecond time scale. Water networks appear to be a hallmark of key functional states and to play a role in allostery. MD simulations and rigidity theory effectively identify intramolecular and interprotomer allosteric pathways, which drive catalysis.

CONCLUSION: FAcD effectively reacts one substrate at a time. However, the empty half of the dimer plays a key role in sampling subsequent functional states and compensating for entropy penalties to binding. Indeed, subsequent states in the catalytic process appear to be sampled through a conformational selection mechanism, in which the empty protomer plays a key role. MD simulations and rigidity theory help to validate many key ideas associated with sampling of states within the ensemble, allostery, and the role of protein dynamics in catalysis. ∎

Heterogeneous dynamics and structural waters in FAcD. In the apo-state, FAcD has a comparable number of waters and *B*-factor amplitudes in each protomer. Binding of substrate increases *B* factors and causes an egress of water molecules in the empty protomer. Upon S_N2 substitution, there is a decrease in *B* factors and an influx of water molecules that continues upon hydrolysis and product formation.

RESEARCH ARTICLE

ENZYME DYNAMICS

The role of dimer asymmetry and protomer dynamics in enzyme catalysis

Tae Hun Kim,[1]*† Pedram Mehrabi,[2,3]* Zhong Ren,[4,5] Adnan Sljoka,[6] Christopher Ing,[7,8] Alexandr Bezginov,[2] Libin Ye,[1] Régis Pomès,[7,8] R. Scott Prosser,[1,7]‡§ Emil F. Pai[2,3,7,9]‡§

Freeze-trapping x-ray crystallography, nuclear magnetic resonance, and computational techniques reveal the distribution of states and their interconversion rates along the reaction pathway of a bacterial homodimeric enzyme, fluoroacetate dehalogenase (FAcD). The crystal structure of apo-FAcD exhibits asymmetry around the dimer interface and cap domain, priming one protomer for substrate binding. This asymmetry is dynamically averaged through conformational exchange on a millisecond time scale. During catalysis, the protomer conformational exchange rate becomes enhanced, the empty protomer exhibits increased local disorder, and water egresses. Computational studies identify allosteric pathways between protomers. Water release and enhanced dynamics associated with catalysis compensate for entropic losses from substrate binding while facilitating sampling of the transition state. The studies provide insights into how substrate-coupled allosteric modulation of structure and dynamics facilitates catalysis in a homodimeric enzyme.

E nzymes greatly accelerate biochemical reactions by providing a scaffold to bind and recognize substrates ([1]), position catalytic units ([2], [3]), and facilitate the formation of stabilized transition states ([4]). Representative states associated with this process are typically sampled by the substrate-free (apo) enzyme, where cooperative motions often play a role in connecting states and propelling the enzyme along the reaction coordinate pathway ([5]–[8]). This dynamic cooperativity is also key to establishing allosteric pathways between the substrate-binding region(s) and the reaction center, resulting in catalysis and release of product(s) ([9], [10]). In analogy with protein folding, cooperative motions are intrinsically important to catalysis in terms of sampling conformations associated with substrate capture, assembling substrates and surmounting enthalpic and entropic barriers, providing for multiple reaction pathways, and regulating overall catalysis—all while avoiding motions that either are unproductive or give rise to misfolding ([11]). Much of this seminal work on dynamic energy landscapes has focused on monomeric enzymes ([3], [5], [6], [8]). Here, we consider the role of dynamics in a homodimeric enzyme, fluoroacetate dehalogenase (FAcD) from *Rhodopseudomonas palustris*, which cleaves carbon-halogen bonds and, in particular, one of nature's strongest covalent single bonds, the carbon-fluorine bond, generating glycolate (Fig. 1A) ([12], [13]). The cleavage of a carbon-halogen bond is initiated through an S_N2 attack by an aspartate residue, Asp[110], which displaces the halogen, resulting in a covalent ester intermediate, while His[155], Trp[156], and Tyr[219] stabilize the leaving halide. Then His[280] activates a water molecule for ester hydrolysis to generate the product glycolate (fig. S1) ([12]).

The ensemble approach to catalysis

Given the requisite roles of enzymes to recognize and position substrate(s) and facilitate catalysis and product release, the notion of a dynamic conformational ensemble is well accepted ([1]–[3], [14]). Substrate binding can contribute energy toward activation through cooperative processes that allow enhanced sampling of catalytically relevant functional states within this ensemble ([15]–[17]). To advance one's understanding of dynamic allostery in the context of catalysis, one would need to first identify the dominant conformations associated with substrate recognition, catalysis, and product release, as illustrated on a hypothetical free energy profile in fig. S1. In the current study, high-resolution crystal structures of the apo-state, the Asp[110] → Asn (D110N) substrate-bound Michaelis complex, a His[280] → Asn (H280N) glycolyl-enzyme covalent intermediate, and a product-bound state constitute a minimum data set with which to identify the appropriate distribution of states (i.e., the ensemble) via nuclear magnetic resonance (NMR) ([18]). When used on the native enzyme and the functional mutants listed above, it is possible to characterize this ensemble as the reaction ensues.

A key facet of the ensemble involves the connectivity of functional states that arise through cooperative dynamic processes, which we associate with allostery ([19], [20]). Enzymes generally exhibit a wide range of dynamics, ranging from subnanosecond local fluctuations, which relate to the conformational entropy of a given state, to concerted processes spanning tens of microseconds or many milliseconds, which serve to transmit binding or catalytic events across the protein ([21], [22]). Even under conditions where enzymes possess low catalytic rates, there are invariably motions at time scales of picoseconds to many milliseconds that may sample the reaction coordinate pathway but are often futile with regard to the generation of product ([23]). Solution-state NMR can play a major role in providing insights into the above fast processes and the slower cooperative processes, often with atomic resolution ([18], [24]–[26]).

Within the arsenal of NMR relaxation experiments, ^{19}F NMR is very useful in delineating states as well as quantitating collective motions that are perhaps too fast for traditional ^{13}C or ^{15}N relaxation experiments, which reveal motions at millisecond time scales ([27]). Biosynthetic labeling, which commonly involves the substitution of aromatic residues such as tryptophan with their monofluorinated equivalents, is generally relatively nonperturbing, as evidenced by the x-ray crystal structure of 5-fluorotryptophan (5F-Trp)–enriched FAcD (fig. S2A), which overlaps within a root-mean-square deviation (RMSD) of 0.14 Å with wild-type FAcD. Although there are no detectable structural perturbations, subtle effects on binding and catalysis are detected by ^{19}F NMR functional assays and isothermal titration calorimetry (ITC) (fig. S2, C to F). Because ^{19}F NMR chemical shifts are extremely sensitive to subtle differences in van der Waals and electrostatic environments, they often resolve multiple states ([28]). These chemical shift differences also greatly help in the measurement of millisecond or submillisecond dynamics, where traditional ^{15}N or ^{13}C relaxation experiments simply do not register the exchange; as shown in fig. S3, virtually no [15]N Carr-Purcell-Meiboom-Gill (CPMG) relaxation dispersions could be detected for a process deemed by ^{19}F CPMG relaxation dispersion experiments to occur at 4300 s^{−1} (see below). Finally, allosteric pathways are characterized by millisecond dynamics and are therefore typically difficult to validate by all-atom molecular dynamics (MD) simulations. For this reason, to ascertain which residues exhibit correlated motions over 40-μs trajectories, we

[1]Department of Chemistry, University of Toronto, Mississauga, Ontario L5L 1C6, Canada. [2]Department of Medical Biophysics, University of Toronto, Toronto, Ontario M5G 1L7, Canada. [3]Ontario Cancer Institute/Princess Margaret Cancer Centre, Campbell Family Institute for Cancer Research, Toronto, Ontario M5G 1L7, Canada. [4]Department of Chemistry, University of Illinois, Chicago, IL 60607, USA. [5]Renz Research Inc., Westmont, IL 60559, USA. [6]CREST, Japan Science and Technology Agency (JST), Department of Informatics, School of Science and Technology, Kwansei Gakuin University, Japan. [7]Department of Biochemistry, University of Toronto, Toronto, Ontario M5S 1A8, Canada. [8]Program in Molecular Structure and Function, Research Institute, Hospital for Sick Children, Toronto, Ontario M5G 1X8, Canada. [9]Department of Molecular Genetics, University of Toronto, Toronto, Ontario M5S 1A8, Canada.
*These authors contributed equally to this work. †Present address: Program in Molecular Structure and Function, Research Institute, Hospital for Sick Children, Toronto, Ontario M5G 1X8, Canada. ‡These authors contributed equally to this work. §Corresponding author. Email: scott.prosser@utoronto.ca (R.S.P.); pai@hera.med.utoronto.ca (E.F.P.)

used MD simulations as well as rigidity-based transmission allostery (RTA) analysis, which accesses motions at millisecond time scales. In particular, RTA identifies physical pathways between protomers or distinct domains in the protein, which can communicate binding or local conformational changes, thereby connecting states identified by crystallography and NMR.

Dynamic allostery in dimers

Quaternary structure is generally understood to facilitate allosteric regulation (*29*–*31*) and, in some cases, to regulate catalysis through distinct oligomerization states (*32*). Only 19% of bacterial proteins are monomers, whereas homodimers are the most prevalent form with 38% (*33*). Curiously, the dimeric enzyme, FAcD, only catalyzes the transformation of a single substrate molecule at a time, calling into question the role of the dimer. To gain insight, we used freeze-trapping x-ray crystallography (FTX), NMR, and computational

techniques to investigate the distribution and interconversion rates of states along the reaction pathway. Because FAcD catalysis is slow, FTX provides a sense of structural changes occurring during catalysis. High-resolution x-ray crystal structures of the catalysis-affecting mutants listed above provide additional indications of dynamic regions through *B*-factor analysis and changes in the numbers of bound waters for each of these reaction steps, while NMR provides a sense of the extent to which distinct functional states are sampled along the reaction coordinate pathway.

Dimer asymmetry

The crystal structure of apo-FAcD shows a subtle asymmetry in the dimer interface and the region around the active site (Fig. 1B). One protomer is in an open state, which is poised for substrate binding; the other protomer exists in a closed state (fig. S1). This asymmetry persists upon binding, as evidenced by linear trajectories of NMR

chemical shifts during substrate titration (Fig. 2B) and x-ray crystal structures of the D110N Michaelis complex, the H280N covalent intermediate, and the D110N glycolate complex, when obtained by cocrystallizing with substrate (D110N and H280N) or product (D110N) (Fig. 1C and fig. S4, A to D). All these structures reveal a single bound substrate molecule per dimer. The only exception is a H280N covalent intermediate structure, obtained from a crystal grown from a solution with an excessive concentration of substrate (fig. S4E) (*12*), indicating that after nucleophilic substitution in one active site, the second site becomes more accessible. Taken together, these findings suggest that catalysis proceeds through half-of-the-sites reactivity (*34*, *35*), where binding to the second site is prevented at least until nucleophilic substitution has taken place.

Because FAcD exhibits a slow enzymatic rate ($k_{cat} = 1.84$ min^{-1} for wild-type FAcD), we could capture structural changes in the dimer by x-ray
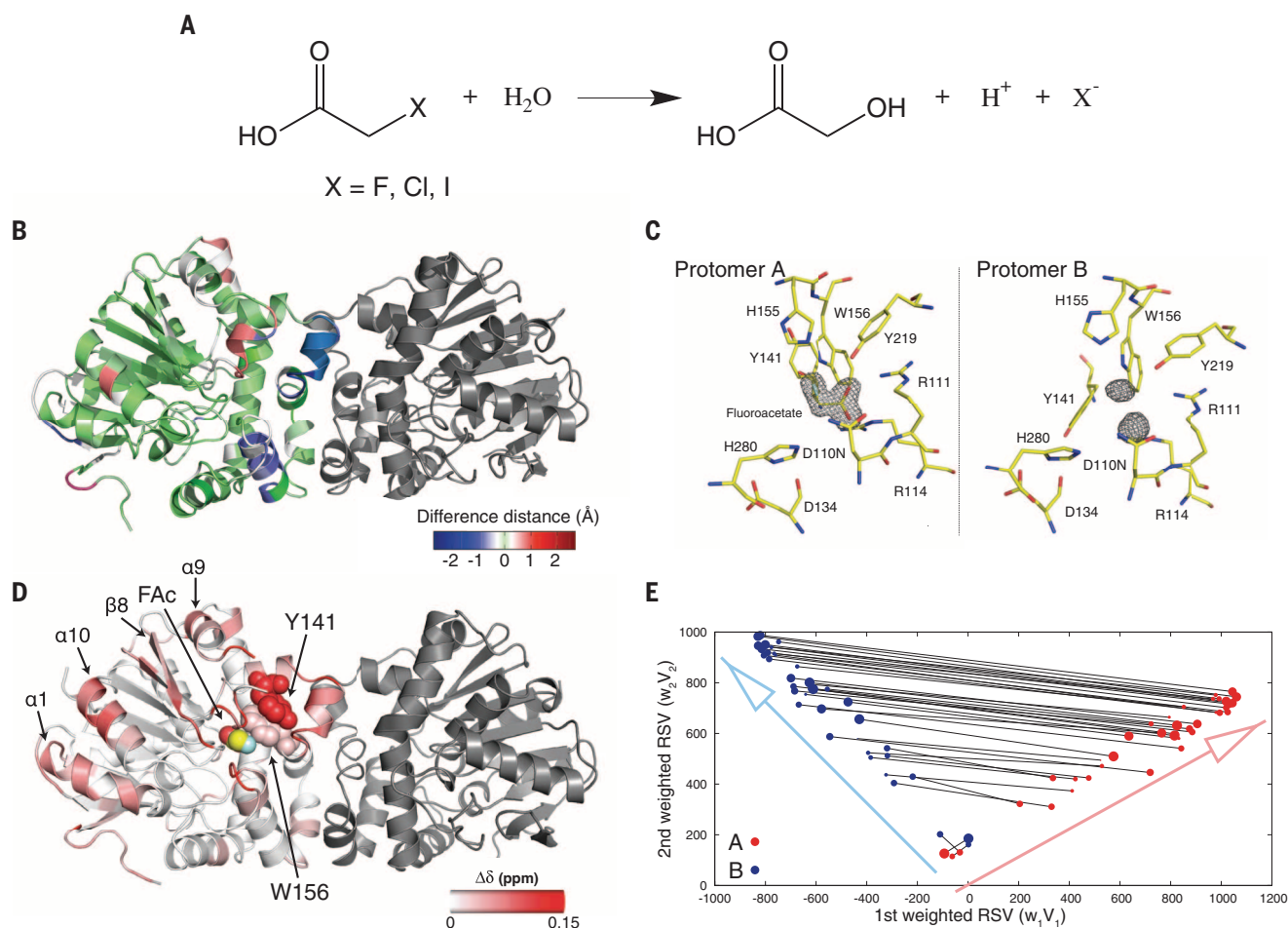
Fig. 1. Structural asymmetry and correlated structural changes in FAcD. (**A**) Chemical reaction catalyzed by FAcD. (**B**) Projection of the difference distance matrix (fig. S6A) between the protomers A and B plotted onto the apo-FAcD crystal structure. (**C**) Michaelis complex of mutant D110N cocrystallized with FAc. (**D**) SPARTA+-predicted chemical shift differences ($\Delta\delta$) between protomers from 38 substrate-soaked crystal structures (*39*). (**E**) Plot of right singular vectors (RSVs) v_1 and v_2, weighted by their corresponding singular

values (w_1, w_2), of 39 protomer pairs from the FTX series including an apo-structure. Coordinates of the two protomers of each dimer in the series are connected by a gray line and are defined by a red and blue dot, representing protomers A and B, as discussed in fig. S6. The diameter of each dot corresponds to the soaking time. Structural changes occurring in protomer A are highly coupled with those in protomer B, but no correlation with soaking time could be established because of stochastic fluctuations arising during soaking.

crystallography after freeze-trapping crystals soaked with substrate for times ranging from 2 to 180 s (*36, 37*). Structural differences between the protomers in the reaction series were analyzed by difference Fourier maps, which were calculated for each protomer of the 38 soaked structures with the ligand-free structure as reference. As shown in Fig. 1, B and D, key asymmetries in the dimer appear to arise in the interface region and in the cap domain, which controls ligand gating. The 78 difference maps of individual protomers were analyzed by singular value decomposition (SVD) analysis to rank decomposed difference components (fig. S5) in order of significance (Fig. 1E, fig. S6, B and C, and fig. S7) (*38*). Although SVD analysis did not yield a time correlation because of stochastic fluctuations that arise during soaking of the ligand, it did reveal highly correlated yet asymmetric structural changes between the protomers during catalysis (Fig. 1E). The two protomers in the same dimer follow very different trajectories marked by arrows for the first few dimensions decomposed by SVD,

which indicates that the difference maps of the two protomers contain unique compositions ($w_i V_i$, where i = 1 to 8).

Dynamic averaging of structural asymmetry

In an effort to correlate the above structural asymmetries with the NMR results, we used SPARTA+ (*39*) to predict the differences between backbone chemical shifts of protomers A and B, averaged over the 38 crystal structures (Fig. 1D) (*39*). Several regions were predicted to exhibit larger chemical shift differences associated with catalysis—namely, the dimer interface region, the cap domain, helices α1, α9, and α10, and the β strand β8 (Fig. 1D). Nonetheless, ^{15}N, ^{1}H, and ^{19}F NMR spectra of the apo-enzyme and substrate-saturated enzyme exhibited a single set of resonances (Fig. 2), which implies that these structural asymmetries are dynamically averaged through conformational exchange. On the basis of predicted differences in ^{15}N and ^{1}H chemical shifts in the regions associated with catalysis, we estimate that the dimer must undergo a conformational exchange between two states (AB ↔ BA) with a conformational exchange rate of k_{ex} ~ 400 s^{-1} as a lower limit in order to dynamically average the expected shift differences (fig. S6D). Given the sensitivity of ^{19}F NMR to subtle differences in van der Waals and electrostatic environments, ^{19}F CPMG relaxation dispersion experiments were performed to characterize potential protomer exchange dynamics in the apo-state (*40, 41*). Although several tryptophan resonances exhibited dispersions (fig. S8A), Trp^{156}, which is located on the dimer interface helix, exhibited a pronounced CPMG dispersion indicative of an exchange rate of k_{ex} = 750 s^{-1} (Fig. 2D and fig. S8B). Thus, the structural asymmetry identified by x-ray crystallography is dynamically averaged in solution.

Probing dynamic asymmetry and protomer exchange during catalysis

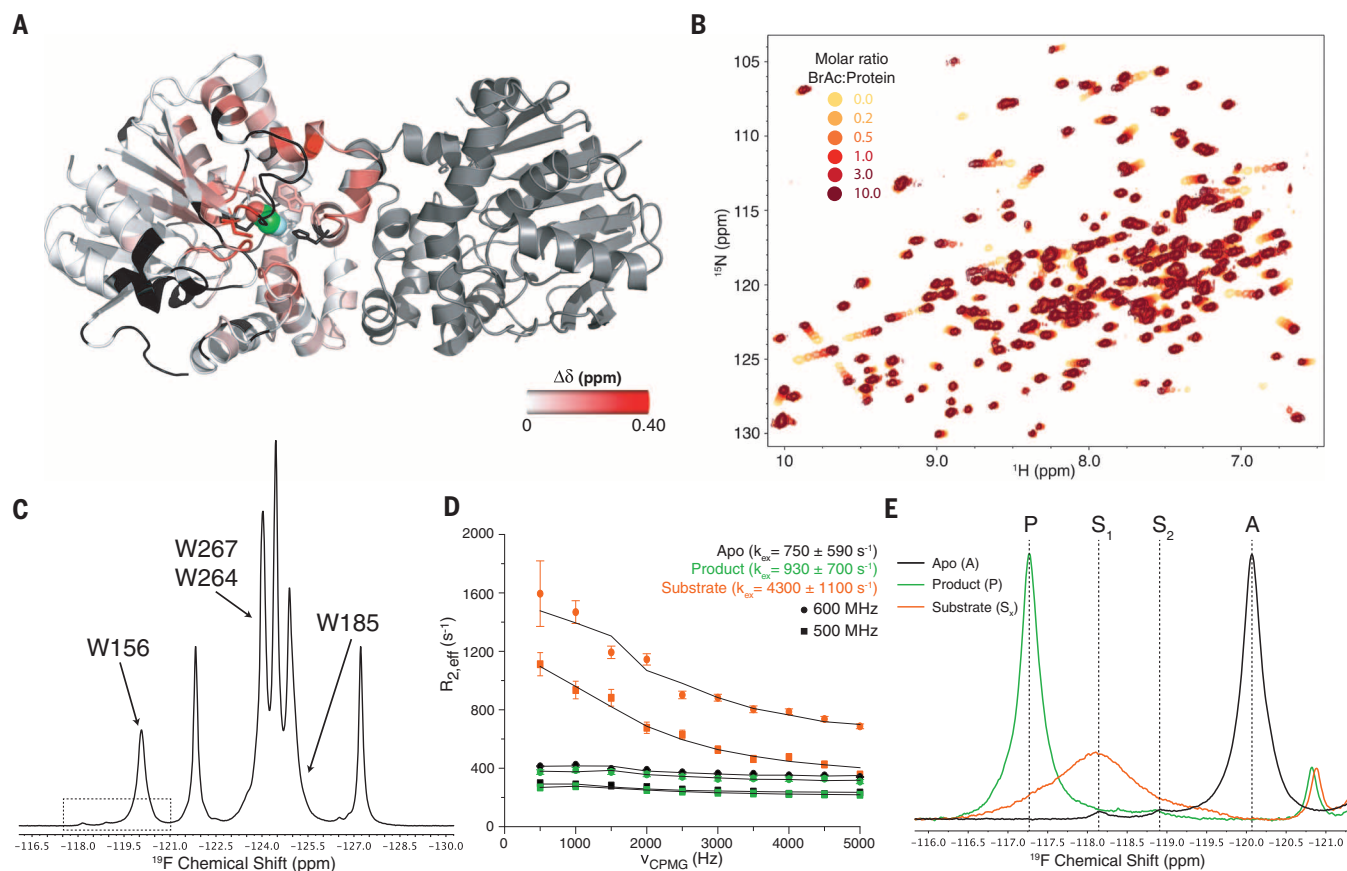To investigate the role of asymmetric conformational exchange between protomers under catalysis,

Fig. 2. Conformational and dynamic changes of FAcD upon titration with substrate analog BrAc observed by ^{15}N,^{1}H HSQC and ^{19}F NMR. (**A**) Chemical shift perturbations resulting from titration of BrAc (B) overlaid onto the Michaelis complex structure. Black regions represent missing peak assignments. (**B**) An expansion of ^{15}N,^{1}H HSQC spectra from a titration series with BrAc; protein ratios range from 0 to 10 at 50°C (see fig. S9B for full spectrum). (**C**) ^{19}F NMR spectrum of 5F-Trp–incorporated FAcD at 50°C. The dashed box showing the major and minor peaks of Trp^{156} is enlarged in Fig. 7B. (**D**) CPMG

relaxation dispersion profiles of Trp^{156} recorded at 600 and 500 MHz. The substrate-bound state (orange) shows dynamics increased by a factor of ~5 relative to the apo- (black) and product-bound states (green). (For an expanded view of CPMG profiles of apo- and product-bound states, see fig. S8B.) (**E**) Trp^{156} shows large chemical shift changes upon addition of substrate analog BrAc (orange) and product (glycolate, in green). Note that the chemical shift of one of the minor peaks (S$_1$) of apo-FAcD matches the "substrate-bound" chemical shift, although without line broadening (dynamics).

we used ^{15}N, ^{1}H, and ^{19}F NMR over a wide concentration range of bromoacetate (BrAc), which conveniently binds and establishes a Michaelis-like intermediate, although without further catalysis as in the case of other haloacetates (Fig. 2, A and B, and fig. S8, C to E). Despite the structural asymmetries in the dimer identified by crystallography, the ^{15}N,^{1}H NMR spectra are indicative of fast protomer conformational exchange over the entire range of BrAc concentrations (Fig. 2B). ^{19}F NMR gave a similar result (Fig. 2E). Of the nine tryptophans in FAcD, all exhibited a single resonance indicating fast protomer conformational exchange dynamics (fig. S8E). The four resonances associated with

Trp^{156}, Trp^{185}, Trp^{264}, and Trp^{267} underwent shifts upon titration with BrAc (fig. S8E). ^{19}F NMR CPMG relaxation dispersion measurements show that addition of the substrate analog BrAc resulted in a protomer conformational exchange rate on the order of 4300 s^{-1}, substantially faster than that in the apo-state (750 s^{-1}) or in glycolate-bound FAcD, which was estimated to be 930 s^{-1} (Fig. 2D).

Resonances that exhibited chemical shift perturbations resulting from the addition of BrAc mapped to the same region of the protein identified by SPARTA+ analysis of the FTX series (Fig. 1D, Fig. 2A, and fig. S9, B to D). In particular, the catalytic site and the interface region

showed the largest chemical shift changes with increasing substrate concentrations, which suggests that conformational changes in the catalytic site of one protomer transmit allosterically to the other protomer via the interface domain (42). This is further corroborated by 40 μs of all-atom MD simulations. Analysis of atomistic trajectories revealed that the dimer interface region and the cap domain have correlated and collective motions extending across the dimer interface (Fig. 3A, fig. S10, and movies S1 to S6). Both symmetric (principal component 1) and asymmetric (principal component 2) collective motions were observed in MD simulations (Fig. 3B). Crystal structures are spread along the asymmetric
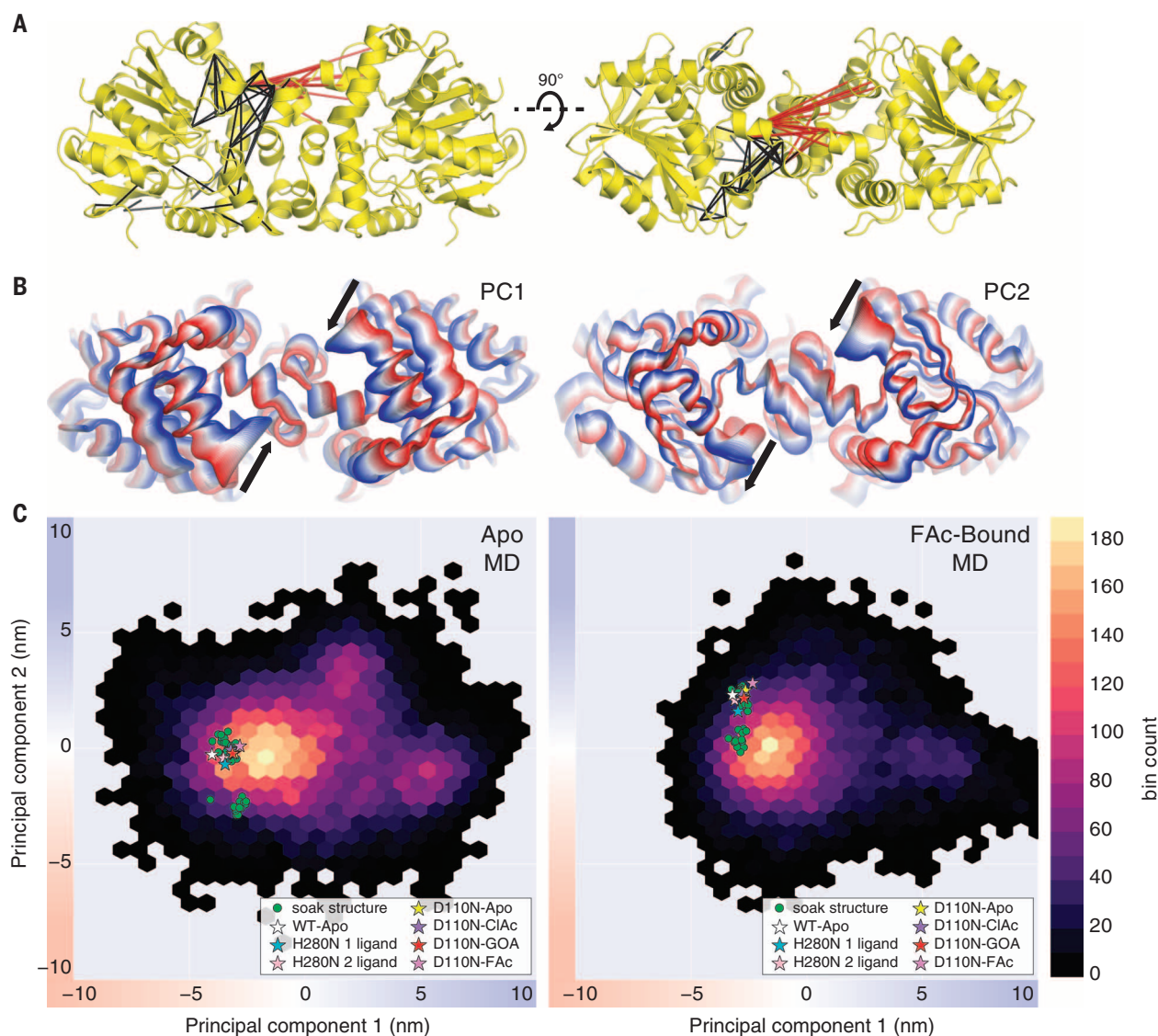
Fig. 3. Cross-correlation of residues and collective motions from MD simulations. (**A**) Side and top views of FAcD depicting mutual information networks of dynamically correlated residues in the apo-state. Black lines indicate intrasubunit correlated residue pairs (threshold of 0.25); red lines indicate intersubunit correlated residue pairs (threshold of 0.2). (**B**) Interpolation between extremes (red and blue) of the first and second principal components of the backbone atom covariance matrix onto the average structure for apo-FAcD simulations. Black arrows indicate overall directions of collective motions in the cap and interface regions of FAcD. (**C**) Two-dimensional projection of the apo- and FAc-bound simulation data sets onto their respective first and second principal components. The colors of the two-dimensional histogram represent the likelihood of observing a simulation snapshot along a collective degree of freedom. Static x-ray crystal structures (stars) and structures obtained from FTX experiments (circles) are projected onto the principal components of the apo- and FAc-bound data sets, respectively.

collective mode, corroborating the motions observed in FTX (Fig. 3C).

Asymmetry in local dynamics and numbers of crystallographic water molecules

Although dimer asymmetry and fast conformational exchange appear to be hallmarks of FAcD catalysis, there is further evidence from crystallographic B factors that the empty protomer of substrate-bound FAcD undergoes rapid internal fluctuations upon initiation of catalysis. As shown in Figs. 4 and 5, the entropic cost associated with substrate binding to the "active" protomer is compensated by an increase in B factors and a decrease in the number of bound water molecules in the empty protomer. Although the B factors and the number of bound waters of both protomers of apo-FAcD are similar, B factors in the ligand-free protomer of the Michaelis complex are markedly increased, with a corresponding loss of water molecules, whereas those of the ligand-bound protomer are mostly unaltered (Fig. 4, A to C, and Fig. 5). This effect is also observed, albeit to a lesser extent, for the ClAc-bound structure (Fig. 4B and Fig. 5, B and C), whose C-Cl dissociation energy is in fact lower by 30 kcal/mol (43). Note that FAcD has evolved to be optimized for FAc over ClAc, where the catalytic rate is conspicuously lower, in keeping with the presumed correlation between entropic contribution (assessed through B factors and crystallographic water molecules) and catalysis (12). B factors and bound waters of the glycolate-bound protomer were comparable to those of the apo-structure (Fig. 4, A and F, and Fig. 5, B and C).

We emphasize that all crystals are highly isomorphous (fig. S11 and table S1), B-factor values generally only average from 9 to 13 Å^2 for main-chain atoms (with changes reaching 17.5 Å^2), and all comparisons were done at the same resolution, which suggests that the observed changes in B factors are real and significant. Thus, asymmetric binding of substrate to one protomer triggers an increase of local dynamics (42) and an egress of protein-bound waters in the empty protomer. This dynamic asymmetry is also observed in covalent intermediate states, in cases where only one of the catalytic sites undergoes a reaction (Fig. 4D and Fig. 5, B and C). In contrast, when both catalytic sites contain the ester intermediate, the protomers exhibit B-factors and numbers of tightly bound waters comparable to those of the apo-state (Fig. 4E and Fig. 5, B and C). The empty protomer becomes dynamic only in substrate-bound and covalent intermediate structures in which a catalytic site is engaged and primed for breaking or forming covalent bonds (Fig. 4, B to D). Thus, substrate binding enables an increase in empty protomer dynamics, which compensates for entropy losses from substrate binding, facilitates sampling of conformations poised to adopt the transition state, and lowers the free energy of the activation barrier through the allosteric network across the dimer.

Interprotomer allosteric pathways

Our x-ray and NMR studies establish that binding of a single substrate molecule to the FAcD dimer initiates a pronounced conformational exchange between protomers on a submillisecond

time scale (i.e., 4300 s^{-1}), which is accompanied by increased disorder in the empty protomer. To identify an allosteric transmission pathway between the substrate binding site of one protomer and the dynamic regions of the empty protomer, we used an RTA algorithm (based on rigidity theory and an extension of the FIRST method) (44–46). The RTA algorithm predicts the extent to which a local mechanical perturbation of rigidity (mimicking ligand binding) at one region can propagate and be allosterically transmitted to another (remote) region. Computationally, the RTA algorithm calculates the number of conformational degrees of freedom at the interface region before and after perturbation of the rigidity of the substrate-binding region (and any consequent transmission in degrees of freedom) is obtained. Mechanically, if two sites are in rigidity-based allosteric communication (i.e., transmit a change in degrees of freedom), then a change in conformation (e.g., as caused by binding) at one site of the network will induce a change in conformation at the second site (47).

The FIRST method makes use of the x-ray crystal structure to generate a constraint network (graph), where the protein is viewed in terms of vertices (atoms) and edges (i.e., covalent bonds, electrostatic bonds, hydrogen bonds, and hydrophobic contacts). Hydrogen bonds are then ranked in terms of overall strength according to local donor-hydrogen-acceptor geometry, and hydrogen bonds weaker than a selected cutoff are ignored. Using a pebble game algorithm (45), the network can be decomposed into rigid clusters and flexible regions, enabling an evaluation of nontrivial degrees of freedom throughout the
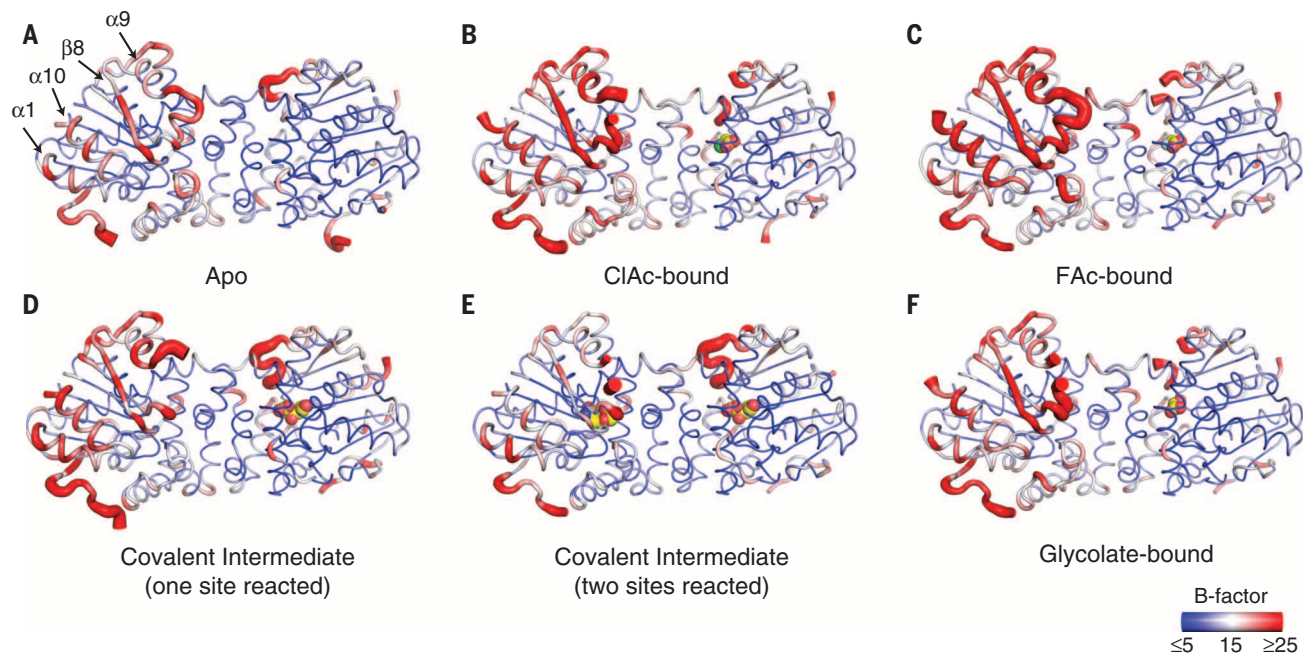
Fig. 4. Heterogeneous dynamics in the dimer at key catalytic steps. Crystallographic B factors are indicated by color, from blue to red, and via a putty tube representation. (**A**) Apo-structure of FAcD (D110N). (**B** and **C**) Michaelis complexes of FAcD (D110N) with substrates ClAc (B) or FAc (C). (**D** and **E**) Covalent ester intermediates with only one catalytic site occupied (D) or both catalytic sites reacted (E). In the case of the singly bound FAc or ester intermediate structures, B factors in the empty protomers are considerably higher. (**F**) B factors in the product glycolate-bound state are notably lower than the FAc-bound state (C).

protein. Substrate binding would typically establish additional constraints at the binding site, which should lead to changes in flexibility elsewhere in the enzyme, thereby contributing to allosteric transmission. FIRST rigid cluster decomposition analysis shows that apo-FAcD consists predominantly of a single large rigid region (indicated in blue in Fig. 6A) spanning the dimer interface. The addition of substrate results in several rigid clusters (designated by color in Fig. 6A) and flexible connections (shown in gray), demonstrating an increase in conformational entropy in the empty protomer.

The RTA algorithm analysis indicates that the transmission of conformational degrees of freedom from the catalytic site in one protomer to the interface region of the empty protomer (Fig. 6B) occurs by allosteric transmission through networks. Thus, computational analysis of allosteric transmission in all three states (i.e., the apo-, Michaelis, and glycolate-bound structures) suggests that there is indeed an underlying allosteric pathway, which extends from the substrate-binding site to the second protomer. Red and green lines represent the hydrogen bond energy cutoffs corresponding to the maximum possible transmission of degrees of freedom and the onset of allosteric transmission for the apo- and ligand-bound dimer structures. In addition, this analysis indicates that less energy is required for allosteric communication between protomers

in the Michaelis complex structure relative to the apo- and the glycolate-bound structures (Fig. 6B) ([44], [48]).

Conformational selection and the reaction coordinate pathway

A key tenet often associated with protein action involves the notion of conformational selection, which in the context of enzymes posits that the ground-state apo-conformer (T state) samples the substrate-bound conformer (R state), even in the absence of substrate ([49]). Substrate binds to the R conformer and thus initiates catalysis. In principle, subsequent steps along the reaction coordinate pathway may also be sampled in a similar manner ([6]). Evidence for such coexistence of states in FAcD is found by both crystallography and ^{19}F NMR. In particular, Tyr^{141} adopts distinct major and minor conformations in each protomer of the apo-FAcD crystal structure, representing two distinct states of the dimer (Fig. 7A). In one protomer (A, whose minor conformer is poised for substrate binding), the tyrosine ring either is positioned away from Trp^{156} in the major conformation or forms π-stacks with Trp^{156} in the minor conformation. In the other protomer (B, whose catalytic site is empty), the side-chain torsion angles χ_1 of the major and minor conformations of Tyr^{141} differ by 19°. Moreover, on the basis of similarities in Tyr^{141} and Trp^{156} side-chain torsion angles in substrate-bound FAcD

(Fig. 7, C and D), we conclude that the minor conformation of protomer A and that of protomer B are coincident in the apo-protein (i.e., there are a total of two states of the apo-protein rather than four).

Consistent with the crystallography results, ^{19}F NMR of apo-FAcD reveals two distinct minor resonances for Trp^{156} with equal areas (i.e., 0.25% that of the major peak) downfield from the corresponding major peak (Fig. 7B). The chemical exchange saturation transfer (CEST) profile shows that the two minor peaks are in slow exchange with the Trp^{156} major peak (Fig. 7B) ([50]). Moreover, the corresponding minor state is represented through additional resonances with equivalent intensities, as shown in fig. S12, which suggests that the minor peaks associated with Trp^{156} signify a global conformational change. Analysis of the Cl$^-$-bound crystal structure (5K3C) and ^{19}F NMR spectra of Trp^{156} → His (W156H) mutant and wild-type FAcD in the presence of NaCl shows that the two minor peaks arise from the distinct minor conformations of Tyr^{141} in each protomer associated with the substrate-bound like state in the apo-form; ring current effects from Tyr^{141} to Trp^{156} make it possible to observe this minor state by ^{19}F NMR (figs. S13 and S14). The ^{19}F NMR resonance was definitively assigned to Trp^{156} through control ^{19}F NMR spectra of the W156H mutant and additional experiments involving the H280N mutant and different ligands,
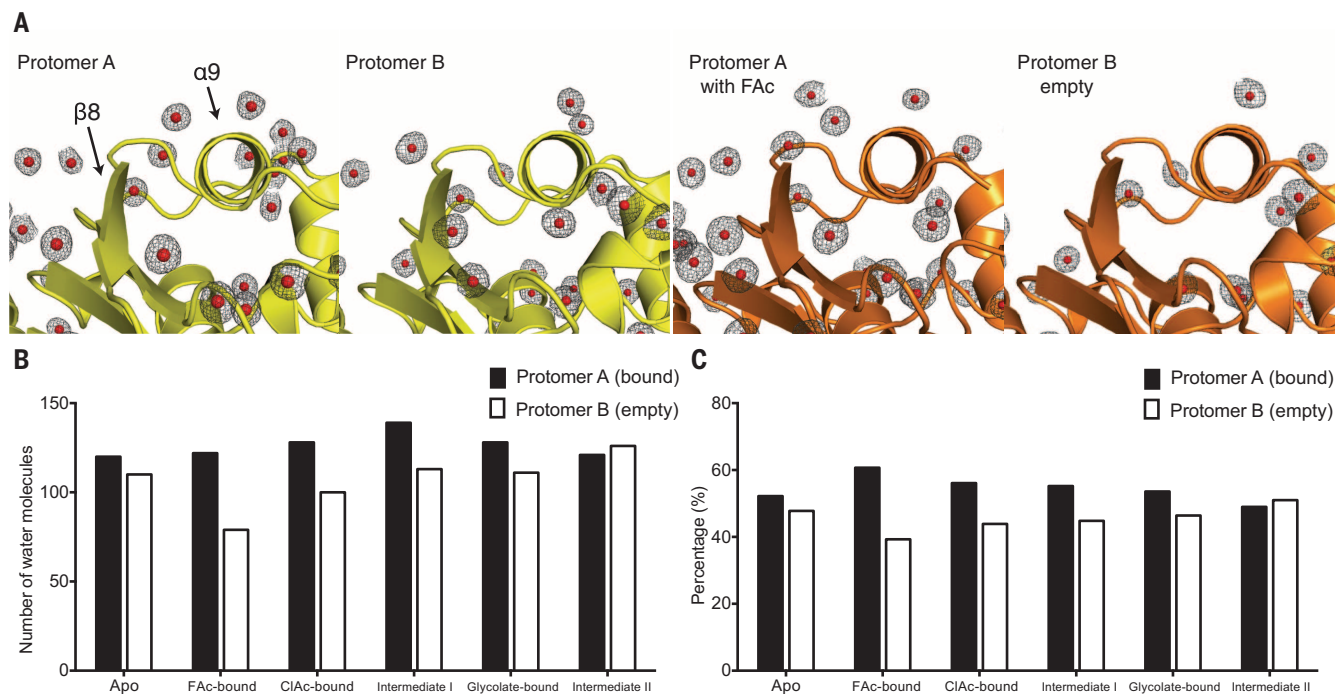
Fig. 5. Distribution of water molecules bound to crystalline FAcD. (**A**) $2F_{obs} - F_{calc}$ electron densities interpreted as water molecules located within 2.8 Å of the next FAcD atom are shown as gray mesh at 1.0σ cutoff. In the FAc-bound structure, the distribution becomes quite asymmetric because of a considerable decrease of water molecules in protomer B, especially around helix α9 and strand β8 of the unbound protomer. Note that these water-depleted regions also exhibit chemical shift perturbations and increased B

factors in the presence of substrate (Figs. 2A and 4). (**B**) Bar graph of number of bound water molecules within 2.8 Å of protomers in the apo- and FAc-bound structures. The apo-structure has similar numbers of water molecules in each protomer. The FAc-bound structure reveals a loss of ~30 water molecules surrounding the ligand-free protomer. (**C**) Bar graph of the same data shown in (B) but as percentages of the total number of tightly bound water molecules.

as described in fig. S13. The minor state observed by ¹⁹F NMR is corroborated by the residual electron density around Tyr¹⁴¹ in the crystal structure (Fig. 7A). Fast protomer conformational exchange of the ground state of apo-FacD—or, indeed, that of the subsequent Michaelis complex, covalent intermediate, and product-bound states—prevents the detection of gross asymmetries under solution conditions. However, the minor state of apo-FAcD, representing the conformation poised for substrate binding, is clearly asymmetric and long-lived, as evidenced by the absence of exchange broadening and the absence of magnetization transfer between minor peaks (Fig. 7B and fig. S8F).

The Michaelis complex and product-bound crystal structures show that the minor conformation associated with the apo-state is predominant upon addition of ligand, with no residual electron densities detected (Fig. 7, C and D, fig. S12). ¹⁹F NMR spectra similarly reveal that the minor (bound-like) state of the apo-enzyme is predominant in the Michaelis complex and glycolate-bound structures (Fig. 2E). The presampling of the bound-like state in the apo-form suggests a conformational selection mechanism in substrate binding (3). In keeping with x-ray crystallography, which showed that the minor state of Tyr¹⁴¹ as found in the apo-form is stabilized in the Michaelis complex, ¹⁹F NMR reveals a clear shift of the major resonance of Trp¹⁵⁶ to one of the minor peaks upon addition of BrAc (Fig. 2E). Thus, the minor state of apo-FAcD represents the substrate-bound–like state, is presampled with

a 0.5% population, and exhibits a lifetime on the order of seconds or longer in the absence of substrate (6). ¹⁹F NMR also shows evidence for sampling of the apo-like ground state (~8% population, represented by a resonance at –120.8 ppm) upon addition of saturating amounts of BrAc (substrate analog) and glycolate (product), in coexistence with the major peak (–118.0 ppm). In this case, the major peak exhibits notable exchange broadening, whereas the major peak resulting from the addition of glycolate does not show line broadening (Fig. 2E).

¹⁹F NMR spectra in the presence of BrAc (Fig. 2E) and crystallographic data also provide evidence for sampling of sequential catalytic states via a conformational selection mechanism, albeit on a faster time scale. Like the apo-form, the Michaelis complex also exhibits structural asymmetry with respect to Tyr¹⁴¹, adopting π-stacked and skewed conformations in the bound and the empty protomers, respectively (Fig. 7C). The π-stacked Tyr¹⁴¹ conformation of the bound protomer (protomer A) is positioned to accommodate the substrate and is also primed for the initial S_N2 nucleophilic substitution. Interestingly, the empty protomer (protomer B) adopts a conformation that is remarkably similar to the covalent intermediate conformation of protomer A, as evidenced by the overlaid crystal structures of the empty protomer (B) in the Michaelis complex and the H280N covalent intermediate (Fig. 7, E and F). This suggests that the intermediate conformation of the reacted protomer (A) is presampled in the empty

protomer of the Michaelis complex. Furthermore, the crystal structures of the occupied protomer (A) of the H280N covalent intermediate and the minor conformation of protomer B in the apo-structure overlay well with each other, suggesting the intermediate conformation is also presampled in the absence of substrate (Fig. 7F, right). Thus, the functional states associated with catalysis (namely, substrate recognition, complex formation, facilitation of S_N2 substitution, and hydrolysis) are elegantly sampled in a sequential fashion via the asymmetric dimer (6). In this case, sampling of the bound-like state is very slow for apo-FAcD, whereas sampling of the intermediate state via the Michaelis intermediate occurs on a submillisecond time scale, as evidenced by ¹⁹F NMR CEST and CPMG experiments, respectively (see below).

The role of dynamics and quaternary structure in catalysis

Although some degree of protein dynamics is generally needed for enzymes to bind substrate and release product, there is debate concerning the relative role of protein dynamics in the chemical step (5, 51–57). It has been suggested that dynamics and flexibility are key to enzyme catalysis and facilitate the chemical step by sampling weakly populated catalytically competent states (52, 55). However, some computational studies argue that the contribution of protein dynamics to the chemical step is minimal and that electrostatic preorganization is the major driving
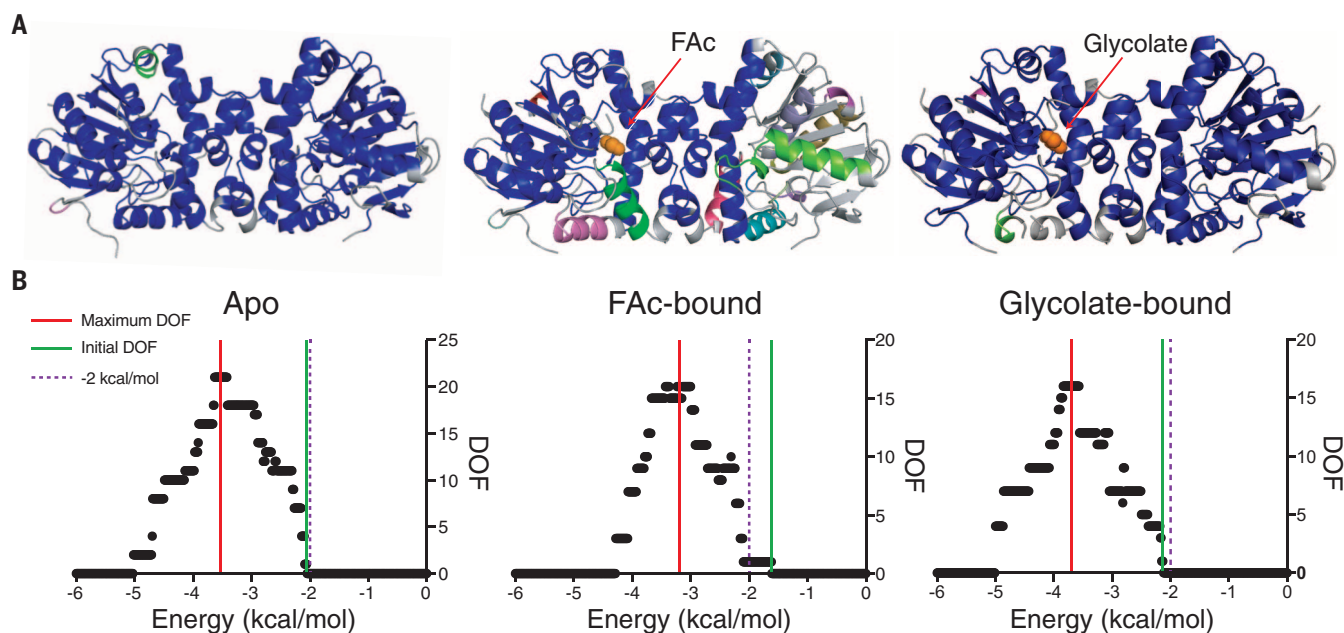
Fig. 6. Computational analyses using rigidity-based transmission models.
(**A**) Computational rigidity predictions with FIRST. Rigid cluster decompositions at an energy cutoff of −2 kcal/mol [purple dashed line in (B)] shows that the Michaelis complex is composed of several rigid clusters (designated by color) and flexible connections (gray), whereas the apo- and the glycolate-bound structures each consist predominantly of a single large rigid region (blue). (**B**) The trans-

mission of conformational degrees of freedom (DOF) from the catalytic site in one protomer to the interface region of the empty protomer (i.e., a change in rigidity at site one propagating to modify rigidity at site two) indicates the presence of rigidity-based allostery between the two protomers. Red and green lines show the hydrogen bond energy cutoffs corresponding to the maximum possible transmission of degrees of freedom and the onset of allosteric transmission, respectively.

force of catalysis ([53], [54]). We revisit this issue in the context of the dimeric enzyme. One hallmark of FAcD is that a subtle structural asymmetry persists in crystal structures of the apo-enzyme, Michaelis complex, covalent intermediate, and product-bound dimer. Moreover, this asymmetry becomes more pronounced as catalysis proceeds, returning to lower values in the product complex. NMR reveals a clear exchange of protomer conformations (AB ↔ BA) on a millisecond time scale ($750 \, s^{-1}$) associated with the ground-state apo-form, whereas the sparsely populated substrate-

bound–like state undergoes no such exchange in the absence of substrate (Fig. 8, I and II). Binding of a single substrate shifts the equilibrium to the bound state and, remarkably, brings about a considerably faster and more pronounced conformational exchange between binding-competent and intermediate states on a submillisecond time scale (Fig. 8, III and IV). This would have the advantage of compensating for entropy losses associated with binding the substrate, providing a route for sampling the covalent intermediate state on a faster time scale and enabling catalysis.

Upon establishing the covalent intermediate (Fig. 8, V), fast internal empty protomer dynamics may also facilitate sampling of conformations that allow attack by an activated water molecule to complete hydrolysis (Fig. 8, VI and VII) and product release. In other words, fast conformational exchange between protomers and strong allosteric coupling facilitate sampling of multiple states, along a pathway that allows the transition state to be sampled with a higher probability. B factors and protein-bound water molecules also contribute to our understanding of the role of dynamics, where a
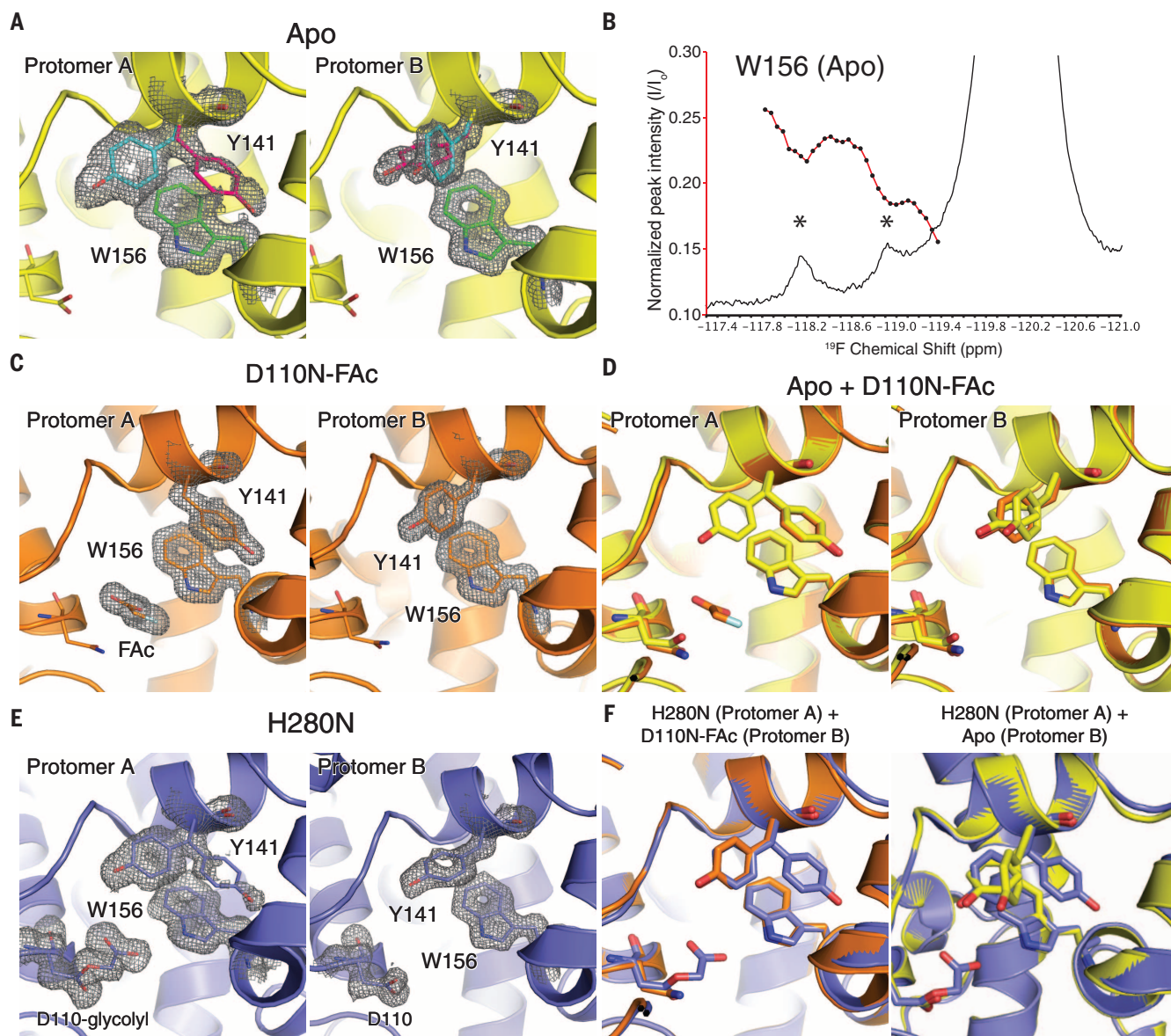
Fig. 7. Crystallographic and spectroscopic evidence of conformational selection. (**A**) $2F_{obs} - F_{calc}$ electron density maps representing the major (cyan) and minor (magenta) conformations of Tyr[141] in crystals of apo-FAcD (5K3D). The cutoff levels for the electron density displayed are 0.3σ and 1.1σ for protomers A and B, respectively. (**B**) Downfield region of the ^{19}F NMR spectrum of apo-FAcD, showing the minor peaks of Trp[156], marked by asterisks. Line widths of deconvolved minor peaks are 73 Hz (left peak) and 92 Hz (right peak). The CEST profile showing the peak intensity of Trp[156] is displayed as a function

of low-power saturation frequency (red trace). Chemical shifts of the troughs match those of the minor peaks. (**C** and **E**) The $2F_{obs} - F_{calc}$ maps of the FAcD active site in the Michaelis complex with FAc [5SWN (C)] and the covalent intermediate [5K3F (E)], showing residues Tyr[141] and Trp[156], glycolyl, and bound ligand as sticks. (**D**) Superposition of the apo-form (5K3D) and the Michaelis complex with FAc (5SWN). (**F**) Crystal structures of the apo-form (5K3D) overlaid with the Michaelis complex with FAc (5SWN, left) and the covalent intermediate (5K3F, right), showing comparable side-chain conformations.

clear enhancement in local motions and changes in the numbers of bound water molecules are seen during catalysis, albeit in domains associated with the empty protomer.

The asymmetry in local dynamics observed during catalysis suggests an advantage for oligomers over monomeric enzymes. In particular, the substrate-bound protomer is able to adopt an optimal pose for efficient catalysis while the empty protomer facilitates the reaction through increased dynamics, for purposes of entropic compensation and sampling of the transition state via tight allosteric coupling between protomers. In addition, the empty protomer appears to serve an additional role with regard to conformational selection and sampling of successive functional states along the reaction coordinate pathway. In particular, the covalent intermediate conformation is sampled by the empty protomer of the Michaelis complex on a rapid time scale upon binding of substrate (4300 s^{-1}). In contrast, the bound-like state of apo-FAcD is sampled on a very slow time scale (seconds). Thus, conformational selection in the dimer essentially knits together key functional states at every point along the reaction coordinate pathway and facilitates overall catalysis by sampling these intermediates.

Despite the increased dynamics upon binding of substrate, there is a large discrepancy between the enzymatic catalytic rate (1.84 min^{-1}) and the time scale of protein dynamics (nanosecond to submillisecond). The catalytic rate is, of course, dependent on a sequence of events

involving alignment of substrate, formation of the covalent intermediate, and a specific attack via an activated water molecule in a unique excited-state pose, all of which may involve many cooperative and noncooperative processes on the part of the enzyme and substrate, prior to attaining the transition state, whereupon the final chemical step may take place on a time scale of femtoseconds or faster. Protein dynamics are thus essential to facilitating overall catalysis, although the experiments described herein do not allow us to interrogate the chemical step.

The role of water networks in stabilizing functional states

We emphasize that the structural asymmetry observed by crystallography, and indeed the differences in structure between distinct functional states of the enzyme (apo-, Michaelis, covalent intermediate, and product), are quite subtle. RMSD differences between the corresponding backbone atoms of the apo-, Michaelis complex, covalent intermediate, and product-bound forms of FAcD are less than 0.3 Å. On the other hand, the presence of bound water networks differs considerably between these functional states, emphasizing the key role of water networks in establishing stable states along the reaction coordinate pathway. This theme of water networks has been repeated in several other recent studies, including the adenosine A_{2A} G protein–coupled receptor (GPCR) (58), where water networks represent a key facet of the activation switch; hemoglobin,

where 60 water molecules are involved in stabilizing the R state upon binding by oxygen (59); and a common hub protein, calmodulin, where the protein bound-like state is sampled on a millisecond time scale and is distinguished by the loss of a network of bound water molecules (60). Water networks present obvious advantages from the perspective of (i) stabilizing states via enthalpic or entropic means, and (ii) establishing long-range dynamic allosteric networks in the case of enzymes, GPCRs, and proteins such as calmodulin that participate in signaling pathways through protein-protein interactions.

Conclusions

Our findings illustrate how half-of-the-sites reactivity in a homodimeric enzyme is regulated by a dynamic allosteric pathway and conformational selection mechanism. Crystallographic and spectroscopic signatures of the apo-enzyme, Michaelis complex, covalent intermediate, and product-bound dimer reveal a subtle structural asymmetry. At any instance, one of the two protomers in the apo-enzyme is primed for ligand binding (Fig. 8, I and II). An asymmetric bound-like state, which is presampled by the apo-enzyme, becomes the dominant state upon binding of substrate, whereupon protomer exchange dynamics is reinforced through allosteric pathways emerging from the substrate-binding site of the ligand-containing protomer and crossing the dimer interface (Fig. 8) (61). Subsequent functional states are also sampled via the dimeric
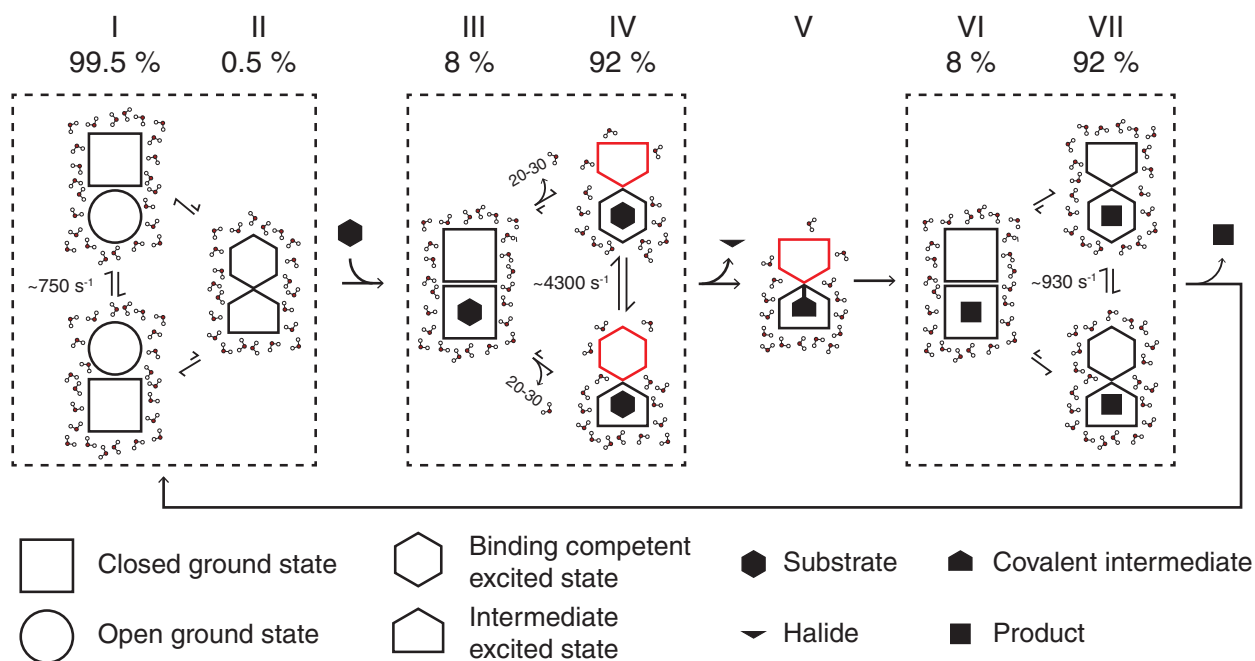
Fig. 8. Proposed mechanistic scheme for FAcD catalysis. In the apo-state, FAcD undergoes fast exchange between two heterogeneous ground states (I) but rarely presamples a long-lived excited state (II). Upon substrate binding, the excited state becomes dominant (IV) with a weakly populated ground state (III). The protomer conformational exchange rate of the excited state (IV) increases substantially, while the local dynamics of the empty protomer

(denoted by red polygons) also increase. At the same time, the number of bound waters in the empty protomer decreases (IV, V). After formation of the ester intermediate, the dynamic empty protomer becomes accessible to substrate and can potentially initiate catalysis (V). Upon formation of product, the conformational exchange rate and the asymmetry in protomer dynamics diminish to a level comparable to that of the apo-state (VI, VII).

enzyme, in a manner consistent with conformational selection. In particular, the empty protomer of the Michaelis intermediate adopts a conformation that closely resembles the bound protomer of the covalent intermediate. The catalytic intermediates display considerable changes in local dynamics and bound water networks, largely in the ligand-free protomer, leading to pronounced asymmetry between the protomers. This increase in configurational entropy and corresponding increased protomer conformational exchange and domain-specific dynamics likely lowers the activation free energy barrier and drives sampling of the transition state. This detailed mechanism provides insights into how substrate-coupled allosteric modulation of structure and dynamics may facilitate catalysis in a homodimeric enzyme.

REFERENCES AND NOTES

1. D. D. Boehr, R. Nussinov, P. E. Wright, The role of dynamic conformational ensembles in biomolecular recognition. *Nat. Chem. Biol.* **5**, 789–796 (2009). doi: 10.1038/nchembio.232; pmid: 19841628

2. D. E. Koshland, Application of a theory of enzyme specificity to protein synthesis. *Proc. Natl. Acad. Sci. U.S.A.* **44**, 98–104 (1958). doi: 10.1073/pnas.44.2.98; pmid: 16590179

3. R. V. Agafonov, C. Wilson, R. Otten, V. Buosi, D. Kern, Energetic dissection of Gleevec's selectivity toward human tyrosine kinases. *Nat. Struct. Mol. Biol.* **21**, 848–853 (2014). doi: 10.1038/nsmb.2891; pmid: 25218445

4. L. Pauling, Nature of forces between large molecules of biological interest. *Nature* **161**, 707–709 (1948). doi: 10.1038/161707a0; pmid: 18860270

5. K. A. Henzler-Wildman et al., Intrinsic motions along an enzymatic reaction trajectory. *Nature* **450**, 838–844 (2007). doi: 10.1038/nature06410; pmid: 18026086

6. D. D. Boehr, D. McElheny, H. J. Dyson, P. E. Wright, The dynamic energy landscape of dihydrofolate reductase catalysis. *Science* **313**, 1638–1642 (2006). doi: 10.1126/science.1130258; pmid: 16973882

7. O. F. Lange et al., Recognition dynamics up to microseconds revealed from an RDC-derived ubiquitin ensemble in solution. *Science* **320**, 1471–1475 (2008). doi: 10.1126/science.1157092; pmid: 18556554

8. J. S. Fraser et al., Hidden alternative structures of proline isomerase essential for catalysis. *Nature* **462**, 669–673 (2009). doi: 10.1038/nature08615; pmid: 19956261

9. Z. H. Foda, Y. Shan, E. T. Kim, D. E. Shaw, M. A. Seeliger, A dynamically coupled allosteric network underlies binding cooperativity in Src kinase. *Nat. Commun.* **6**, 5939 (2015). doi: 10.1038/ncomms6939; pmid: 25600932

10. D. Oyen, R. B. Fenwick, R. L. Stanfield, H. J. Dyson, P. E. Wright, Cofactor-mediated conformational dynamics promote product release from *Escherichia coli* dihydrofolate reductase via an allosteric pathway. *J. Am. Chem. Soc.* **137**, 9459–9468 (2015). doi: 10.1021/jacs.5b05707; pmid: 26147643

11. G. D. Rose, P. J. Fleming, J. R. Banavar, A. Maritan, A backbone-based theory of protein folding. *Proc. Natl. Acad. Sci. U.S.A.* **103**, 16623–16633 (2006). doi: 10.1073/pnas.0606843103; pmid: 17075053

12. P. W. Y. Chan, A. F. Yakunin, E. A. Edwards, E. F. Pai, Mapping the reaction coordinates of enzymatic defluorination. *J. Am. Chem. Soc.* **133**, 7461–7468 (2011). doi: 10.1021/ja200277d; pmid: 21510690

13. P. Goldman, The carbon-fluorine bond in compounds of biological interest. *Science* **164**, 1123–1130 (1969). doi: 10.1126/science.164.3884.1123; pmid: 4890091

14. A. De Simone, F. A. Aprile, A. Dhulesia, C. M. Dobson, M. Vendruscolo, Structure of a low-population intermediate state in the release of an enzyme product. *eLife* **4**, 737 (2015). doi: 10.7554/eLife.02777; pmid: 25575179

15. A. Cooper, D. T. F. Dryden, Allostery without conformational change. A plausible model. *Eur. Biophys. J.* **11**, 103–109 (1984). doi: 10.1007/BF00276625; pmid: 6544679

16. Q. Cui, M. Karplus, Allostery and cooperativity revisited. *Protein Sci.* **17**, 1295–1307 (2008). doi: 10.1110/ps.03259908; pmid: 18560010

17. H. N. Motlagh, J. O. Wrabl, J. Li, V. J. Hilser, The ensemble nature of allostery. *Nature* **508**, 331–339 (2014). doi: 10.1038/nature13001; pmid: 24740064

18. A. Sekhar et al., Thermal fluctuations of immature SOD1 lead to separate folding and misfolding pathways. *eLife* **4**, e07296 (2015). doi: 10.7554/eLife.07296; pmid: 26099300

19. S.-R. Tzeng, C. G. Kalodimos, Dynamic activation of an allosteric regulatory protein. *Nature* **462**, 368–372 (2009). doi: 10.1038/nature08560; pmid: 19924217

20. S.-R. Tzeng, C. G. Kalodimos, Protein activity regulation by conformational entropy. *Nature* **488**, 236–240 (2012). doi: 10.1038/nature11271; pmid: 22801505

21. A. J. Wand, The dark energy of proteins comes to light: Conformational entropy and its role in protein function revealed by NMR relaxation. *Curr. Opin. Struct. Biol.* **23**, 75–81 (2013). doi: 10.1016/j.sbi.2012.11.005; pmid: 23246280

22. A. Neu, U. Neu, A.-L. Fuchs, B. Schlager, R. Sprangers, An excess of catalytically required motions inhibits the scavenger decapping enzyme. *Nat. Chem. Biol.* **11**, 697–704 (2015). doi: 10.1038/nchembio.1866; pmid: 26258763

23. A. Bar-Even, R. Milo, E. Noor, D. S. Tawfik, The moderately efficient enzyme: Futile encounters and enzyme floppiness. *Biochemistry* **54**, 4969–4977 (2015). doi: 10.1021/acs.biochem.5b00621; pmid: 26219075

24. G. Bouvignies et al., Solution structure of a minor and transiently formed state of a T4 lysozyme mutant. *Nature* **477**, 111–114 (2011). doi: 10.1038/nature10349; pmid: 21857680

25. V. Kasinath, K. A. Sharp, A. J. Wand, Microscopic insights into the NMR relaxation-based protein conformational entropy meter. *J. Am. Chem. Soc.* **135**, 15092–15100 (2013). doi: 10.1021/ja405200u; pmid: 24007504

26. S. Grutsch, S. Brüschweiler, M. Tollinger, NMR methods to study dynamic allostery. *PLOS Comput. Biol.* **12**, e1004620 (2016). doi: 10.1371/journal.pcbi.1004620; pmid: 26964042

27. A. Manglik et al., Structural insights into the dynamic process of β₂-adrenergic receptor signaling. *Cell* **161**, 1101–1111 (2015). doi: 10.1016/j.cell.2015.04.043; pmid: 25981665

28. L. Ye, N. Van Eps, M. Zimmer, O. P. Ernst, R. S. Prosser, Activation of the A2A adenosine G-protein-coupled receptor by conformational selection. *Nature* **533**, 265–268 (2016). doi: 10.1038/nature17668; pmid: 27144352

29. L. Freiburger et al., Substrate-dependent switching of the allosteric binding mechanism of a dimeric enzyme. *Nat. Chem. Biol.* **10**, 937–942 (2014). doi: 10.1038/nchembio.1626; pmid: 25218742

30. J. Monod, J. Wyman, J.-P. Changeux, On the nature of allosteric transitions: A plausible model. *J. Mol. Biol.* **12**, 88–118 (1965). doi: 10.1016/S0022-2836(65)80285-6; pmid: 14343300

31. D. E. Koshland Jr., K. E. Neet, The catalytic and regulatory properties of enzymes. *Annu. Rev. Biochem.* **37**, 359–410 (1968). doi: 10.1146/annurev.bi.37.070168.002043; pmid: 4877056

32. T. W. Traut, Dissociation of enzyme oligomers: A mechanism for allosteric regulation. *Crit. Rev. Biochem. Mol. Biol.* **29**, 125–163 (1994). doi: 10.3109/10409239409086799; pmid: 8026214

33. D. S. Goodsell, A. J. Olson, Structural symmetry and protein function. *Annu. Rev. Biophys. Biomol. Struct.* **29**, 105–153 (2000). doi: 10.1146/annurev.biophys.29.1.105; pmid: 10940245

34. M. Castellani et al., Direct demonstration of half-of-the-sites reactivity in the dimeric cytochrome bc1 complex: Enzyme with one inactive monomer is fully active but unable to activate the second ubiquinol oxidation site in response to ligand binding at the ubiquinone reduction site. *J. Biol. Chem.* **285**, 502–510 (2010). doi: 10.1074/jbc.M109.072959; pmid: 19892700

35. D. E. Koshland Jr., The structural basis of negative cooperativity: Receptors and enzymes. *Curr. Opin. Struct. Biol.* **6**, 757–761 (1996). doi: 10.1016/S0959-440X(96)80004-2; pmid: 8994875

36. E. Fiedler et al., Snapshot of a key intermediate in enzymatic thiamin catalysis: Crystal structure of the α-carbanion of (α,β-dihydroxyethyl)-thiamin diphosphate in the active site of transketolase from *Saccharomyces cerevisiae*. *Proc. Natl. Acad. Sci. U.S.A.* **99**, 591–595 (2002). doi: 10.1073/pnas.022510999; pmid: 11773632

37. X. Ding, B. F. Rasmussen, G. A. Petsko, D. Ringe, Direct structural observation of an acyl-enzyme intermediate in the hydrolysis of an ester substrate by elastase. *Biochemistry* **33**, 9285–9293 (1994). doi: 10.1021/bi00197a032; pmid: 8049229

38. Z. Ren et al., Resolution of structural heterogeneity in dynamic crystallography. *Acta Crystallogr. D* **69**, 946–959 (2013). doi: 10.1107/S0907444913003454; pmid: 23695239

39. Y. Shen, A. Bax, SPARTA+: A modest improvement in empirical NMR chemical shift prediction by means of an artificial neural network. *J. Biomol. NMR* **48**, 13–22 (2010). doi: 10.1007/s10858-010-9433-9; pmid: 20628786

40. S. D. Hoeltzli, C. Frieden, Stopped-flow NMR spectroscopy: Real-time unfolding studies of 6-¹⁹F-tryptophan-labeled *Escherichia coli* dihydrofolate reductase. *Proc. Natl. Acad. Sci. U.S.A.* **92**, 9318–9322 (1995). doi: 10.1073/pnas.92.20.9318; pmid: 7568125

41. J. L. Kitevski-LeBlanc, R. S. Prosser, Current applications of ¹⁹F NMR to studies of protein structure and dynamics. *Prog. Nucl. Magn. Reson. Spectrosc.* **62**, 1–33 (2012). doi: 10.1016/j.pnmrs.2011.06.003; pmid: 22364614

42. N. Popovych, S. Sun, R. H. Ebright, C. G. Kalodimos, Dynamically driven protein allostery. *Nat. Struct. Mol. Biol.* **13**, 831–838 (2006). doi: 10.1038/nsmb1132; pmid: 16906160

43. T. Kamachi et al., The catalytic mechanism of fluoroacetate dehalogenase: A computational exploration of biological dehalogenation. *Chemistry* **15**, 7394–7403 (2009). doi: 10.1002/chem.200801813; pmid: 19551770

44. D. J. Jacobs, A. J. Rader, L. A. Kuhn, M. F. Thorpe, Protein flexibility predictions using graph theory. *Proteins Struct. Funct. Bioinf.* **44**, 150–165 (2001). doi: 10.1002/prot.1081

45. D. J. Jacobs, B. Hendrickson, An algorithm for two-dimensional rigidity percolation: The pebble game. *J. Comput. Phys.* **137**, 346–365 (1997). doi: 10.1006/jcph.1997.5809

46. M. V. Chubynsky, M. F. Thorpe, Algorithms for three-dimensional rigidity analysis and a first-order percolation transition. *Phys. Rev. E* **76**, 041135 (2007). doi: 10.1103/PhysRevE.76.041135; pmid: 17994964

47. W. Finbow-Singh, W. Whiteley, Isostatic block and hole frameworks. *SIAM J. Discrete Math.* **27**, 991–1020 (2013). doi: 10.1137/100801044

48. A. Sljoka, thesis, York University (2012).

49. J. Monod, J.-P. Changeux, F. Jacob, Allosteric proteins and cellular control systems. *J. Mol. Biol.* **6**, 306–329 (1963). doi: 10.1016/S0022-2836(63)80091-1; pmid: 13936070

50. S. Forsén, R. A. Hoffman, Study of moderately rapid chemical exchange reactions by means of nuclear magnetic double resonance. *J. Chem. Phys.* **39**, 2892 (1963). doi: 10.1063/1.1734121

51. E. Z. Eisenmesser et al., Intrinsic dynamics of an enzyme underlies catalysis. *Nature* **438**, 117–121 (2005). doi: 10.1038/nature04105; pmid: 16267559

52. G. Bhabha et al., A dynamic knockout reveals that conformational fluctuations influence the chemical step of enzyme catalysis. *Science* **332**, 234–238 (2011). doi: 10.1126/science.1198542; pmid: 21474759

53. A. V. Pisliakov, J. Cao, S. C. L. Kamerlin, A. Warshel, Enzyme millisecond conformational dynamics do not catalyze the chemical step. *Proc. Natl. Acad. Sci. U.S.A.* **106**, 17359–17364 (2009). doi: 10.1073/pnas.0909150106; pmid: 19805169

54. A. J. Adamczyk, J. Cao, S. C. L. Kamerlin, A. Warshel, Catalysis by dihydrofolate reductase and other enzymes arises from electrostatic preorganization, not conformational motions. *Proc. Natl. Acad. Sci. U.S.A.* **108**, 14115–14120 (2011). doi: 10.1073/pnas.1111252108; pmid: 21831831

55. A. Kohen, R. Cannio, S. Bartolucci, J. P. Klinman, Enzyme dynamics and hydrogen tunnelling in a thermophilic alcohol dehydrogenase. *Nature* **399**, 496–499 (1999). doi: 10.1038/20981; pmid: 10365965

56. R. García-Meseguer, S. Martí, J. J. Ruiz-Pernía, V. Moliner, I. Tuñón, Studying the role of protein dynamics in an SN2 enzyme reaction using free-energy surfaces and solvent coordinates. *Nat. Chem.* **5**, 566–571 (2013). doi: 10.1038/nchem.1660; pmid: 23787745

57. A. Warshel, R. P. Bora, Defining and quantifying the role of dynamics in enzyme catalysis. *J. Chem. Phys.* **144**, 180901 (2016). doi: 10.1063/1.4947037; pmid: 27179464

58. W. Liu et al., Structural basis for allosteric regulation of GPCRs by sodium ions. *Science* **337**, 232–236 (2012). doi: 10.1126/science.1219218; pmid: 22798613

59. M. F. Colombo, D. C. Rau, V. A. Parsegian, Protein solvation in allosteric regulation: A water effect on hemoglobin. *Science* **256**, 655–659 (1992). doi: 10.1126/science.1585178; pmid: 1585178

60. J. Hoang, R. S. Prosser, Conformational selection and functional dynamics of calmodulin: A ¹⁹F nuclear magnetic resonance study. *Biochemistry* **53**, 5727–5736 (2014). doi: 10.1021/bi500679c; pmid: 25148136

61. K. Gunasekaran, B. Y. Ma, R. Nussinov, Is allostery an intrinsic property of all dynamic proteins? *Proteins Struct. Funct. Bioinf.* **57**, 433–443 (2004). doi: 10.1002/prot.20232

62. W. Y. Chan *et al.*, Sequence- and activity-based screening of microbial genomes for novel dehalogenases. *Microb. Biotechnol.* **3**, 107–120 (2010). doi: 10.1111/j.1751-7915.2009.00155.x; pmid: 21255311

63. W. Kabsch, XDS. *Acta Crystallogr. D* **66**, 125–132 (2010). doi: 10.1107/S0907444909047337; pmid: 20124692

64. A. J. McCoy *et al.*, Phaser crystallographic software. *J. Appl. Crystallogr.* **40**, 658–674 (2007). doi: 10.1107/S0021889807021206; pmid: 19461840

65. P. Emsley, B. Lohkamp, W. G. Scott, K. Cowtan, Features and development of Coot. *Acta Crystallogr. D* **66**, 486–501 (2010). doi: 10.1107/S0907444910007493; pmid: 20383002

66. A. A. Vagin *et al.*, REFMAC5 dictionary: Organization of prior chemical knowledge and guidelines for its use. *Acta Crystallogr. D* **60**, 2184–2195 (2004). doi: 10.1107/S0907444904023510; pmid: 15572771

67. M. D. Winn *et al.*, Overview of the CCP4 suite and current developments. *Acta Crystallogr. D* **67**, 235–242 (2011). doi: 10.1107/S0907444910045749; pmid: 21460441

68. P. D. Adams *et al.*, PHENIX: A comprehensive Python-based system for macromolecular structure solution. *Acta Crystallogr. D* **66**, 213–221 (2010). doi: 10.1107/S0907444909052925; pmid: 20124702

69. Z. Ren, Reaction trajectory revealed by a joint analysis of protein data bank. *PLOS ONE* **8**, e77141 (2013). doi: 10.1371/journal.pone.0077141; pmid: 24244274

70. M. Sattler, J. Schleucher, C. Griesinger, Heteronuclear multidimensional NMR experiments for the structure determination of proteins in solution employing pulsed field gradients. *Prog. Nucl. Magn. Reson. Spectrosc.* **34**, 93–158 (1999). doi: 10.1016/S0079-6565(98)00025-9

71. L. Shi, L. E. Kay, Tracing an allosteric pathway regulating the activity of the HslV protease. *Proc. Natl. Acad. Sci. U.S.A.* **111**, 2140–2145 (2014). doi: 10.1073/pnas.1318476111; pmid: 24469799

72. F. Delaglio *et al.*, NMRPipe: A multidimensional spectral processing system based on UNIX pipes. *J. Biomol. NMR* **6**, 277–293 (1995). doi: 10.1007/BF00197809; pmid: 8520220

73. B. A. Johnson, R. A. Blevins, NMR View: A computer program for the visualization and analysis of NMR data. *J. Biomol. NMR* **4**, 603–614 (1994). doi: 10.1007/BF00404272; pmid: 22911360

74. W. F. Vranken *et al.*, The CCPN data model for NMR spectroscopy: development of a software pipeline. *Proteins*

Struct. Funct. Bioinf. **59**, 687–696 (2005). doi: 10.1002/prot.20449

75. W. Whiteley, Counting out to the flexibility of molecules. *Phys. Biol.* **2**, S116–S126 (2005). doi: 10.1088/1478-3975/2/4/S06; pmid: 16280617

76. K. Lindorff-Larsen *et al.*, Improved side-chain torsion potentials for the Amber ff99SB protein force field. *Proteins Struct. Funct. Bioinf.* **78**, 1950–1958 (2010). doi: 10.1002/prot.22711

77. W. L. Jorgensen, J. Chandrasekhar, J. D. Madura, R. W. Impey, M. L. Klein, Comparison of simple potential functions for simulating liquid water. *J. Chem. Phys.* **79**, 926 (1983). doi: 10.1063/1.445869

78. A. W. Sousa da Silva, W. F. Vranken, ACPYPE - AnteChamber PYthon Parser interfacE. *BMC Res. Notes* **5**, 367 (2012). doi: 10.1186/1756-0500-5-367; pmid: 22824207

79. J. Wang, W. Wang, P. A. Kollman, D. A. Case, Automatic atom type and bond type perception in molecular mechanical calculations. *J. Mol. Graph. Model.* **25**, 247–260 (2006). doi: 10.1016/j.jmgm.2005.12.005; pmid: 16458552

80. S. Pronk *et al.*, GROMACS 4.5: A high-throughput and highly parallel open source molecular simulation toolkit. *Bioinformatics* **29**, 845–854 (2013). doi: 10.1093/bioinformatics/btt055; pmid: 23407358

81. W. G. Hoover, Canonical dynamics: Equilibrium phase-space distributions. *Phys. Rev. A* **31**, 1695–1697 (1985). doi: 10.1103/PhysRevA.31.1695; pmid: 9895674

82. S. Nosé, A unified formulation of the constant temperature molecular dynamics methods. *J. Chem. Phys.* **81**, 511–519 (1984). doi: 10.1063/1.447334

83. S. Nosé, M. L. Klein, Constant pressure molecular dynamics for molecular systems. *Mol. Phys.* **50**, 1055–1076 (2006). doi: 10.1080/00268978300102851

84. T. Darden, D. York, L. Pedersen, Particle mesh Ewald: An N·log (N) method for Ewald sums in large systems. *J. Chem. Phys.* **98**, 10089 (1993). doi: 10.1063/1.464397

85. U. Essmann *et al.*, A smooth particle mesh Ewald method. *J. Chem. Phys.* **103**, 8577 (1995). doi: 10.1063/1.470117

86. S. Miyamoto, P. A. Kollman, SETTLE: An analytical version of the SHAKE and RATTLE algorithm for rigid water models. *J. Comput. Chem.* **13**, 952–962 (1992). doi: 10.1002/jcc.540130805

87. B. Hess, P-LINCS: A parallel linear constraint solver for molecular simulation. *J. Chem. Theory Comput.* **4**, 116–122 (2008). doi: 10.1021/ct700200b; pmid: 26619985

88. R. T. McGibbon *et al.*, MDTraj: A modern open library for the analysis of molecular dynamics trajectories. *Biophys. J.* **109**, 1528–1532 (2015). doi: 10.1016/j.bpj.2015.08.015; pmid: 26488642

89. C. X. Hernández, mdentropy: v0.2 (2015). doi: 10.5281/zenodo.18859

90. W. Humphrey, A. Dalke, K. Schulten, VMD: Visual molecular dynamics. *J. Mol. Graph.* **14**, 33–38, 27–28 (1996). doi: 10.1016/0263-7855(96)00018-5; pmid: 8744570

91. A. Fiser, A. Sali, Modeller: Generation and refinement of homology-based protein structure models. *Methods Enzymol.* **374**, 461–491 (2003). doi: 10.1016/S0076-6879(03)74020-8; pmid: 14696385

SUPPLEMENTARY MATERIALS

Science

AAAS

Editor's Summary

Working as a pair

Enzymes provide scaffolds that facilitate chemical reactions. Enzyme dynamics often enhance reactivity by allowing the enzyme to sample the transition state between reactants and products. Kim *et al.* explored the role of dynamics in the dimeric enzyme fluoroacetate dehalogenase (see the Perspective by Saleh and Kalodimos). They found that the two protomers are asymmetric, with only one being able to bind substrate at a time. The nonbinding protomer contributed to catalysis by becoming more dynamic to compensate for the entropy loss of its partner.

Science, this issue p. 10.1126/science.aag2355 ; see also p. 247

Article Tools	Visit the online version of this article to access the personalization and article tools: http://science.sciencemag.org/content/355/6322/eaag2355
Permissions	Obtain information about reproducing this article: http://www.sciencemag.org/about/permissions.dtl